

# High-contrast low-dose proton radiography of thin samples at the Tandetron accelerator

Vaclav Olsansky<sup>1,2\*</sup>, Carlos Granja<sup>3</sup>, Cristina Oancea<sup>3</sup>, Pavel Krist<sup>1</sup>, Anna Mackova<sup>1,4</sup>,  
Vladimir Havranek<sup>1</sup> and Jiri Bila<sup>2</sup>

<sup>1</sup>Nuclear Physics Institute Czech Ac. of Sc., p.r.i., Husinec-Rez 130, 250 68 Rez near Prague, Czech Republic

<sup>2</sup>Faculty of Mechanical Engineering, Czech Tech. Univ. in Prague, Technicka 4, 160 00 Prague 6, Czech Republic

<sup>3</sup>Advacam, U Pergamenky 12, 170 00 Prague 7, Czech Republic

<sup>4</sup>Faculty of Science, J. E. Purkinje University, Pasteurova 1, 400 96 Usti nad Labem, Czech Republic

**Abstract.** We investigate the ability of using high-resolution position-sensitive pixel detector and standard non-scanning beams of low-energy protons in air as a flexible tool and simplified technique for density-sensitivity imaging of thin samples. Proton radiography can provide high contrast and low radiation dose delivered to the inspected sample. Density-sensitive contrast response can be provided by a single proton per imaging pixel. For this purpose, we use the silicon semiconductor high-resolution pixel detector Timepix3 to evaluate particle radiography of thin samples with monoenergetic low-energy proton beams from the Tandetron light-ion accelerator. Measurements were performed with various well-defined thin samples. A proton micro beam was used to test and evaluate the technique. Spatial information of the samples is provided by the imaging detector. Density-sensitive contrast is obtained from the measurement of small differences in the deposited energy of transmitted protons across the sample. The transmitted protons are detected with high spatial resolution in the pixel detector. The single particle tracks registered in the detector are analysed by detailed pattern recognition algorithms. Various of these track parameters of spectral response are used for imaging contrast. Resulting proton radiographies for various well-defined thin samples are presented.

## 1 Introduction and Motivation

Use of protons for imaging of objects dates back to the 1960s, when proton radiography was introduced [1]. Depending on the particle energy and the resulting range penetration in the inspected samples together with experimental setup restraints (e.g., vacuum or in-air measurements), several techniques have been developed according to the capabilities provided by delivered particle beams and available radiation detectors [2]. Scanning transmission ion microscopy (STIM) achieved with high-spatial resolution microbeams and

---

\* Corresponding author: [olsansky@ujf.cas.cz](mailto:olsansky@ujf.cas.cz)

conventional single-pad semiconductor diodes measures the deposited energy of transmitted protons and ions through the imaged sample [3-4]. The single-particle sensitivity and deposited energy response give the capability to provide enhanced resolving power of low-contrast structures [3-5]. On the contrary, in conventional radiation imaging, such as in standard X-ray radiography, changes in beam intensity are used for generation of the contrast mechanism [2]. The use of position-sensitive high-sensitivity imaging detectors enables to use the technique with standard non-focused and non-scanning beams which can be more readily accessed including measurements in air. Even a standard radionuclide alpha source, e.g.,  $^{241}\text{Am}$ , can be used [5]. In addition, very few particles, even only one proton per image bin can be sufficient to provide contrast information [6]. A benefit of this approach is that the particle goes through the sample, transferring only a small amount of energy yielding a low fluency of the radiation required to provide imaging information. The image sample can be thus exposed to a lower radiation dose than X-rays, which otherwise require irradiation of large number of quanta per imaging bin many of which are absorbed in the sample.

In this work we develop and evaluate a simple and practical approach with low-energy protons in air using high-resolution semiconductor pixel detectors. The goal is to implement the application of high-sensitivity low energy proton radiography at the Tandatron 4130 MC accelerator at the NPI CAS [7-8].

We use of the new Timepix3 ASIC chip detector [9] for enhanced-contrast density-sensitive radiography of thin samples irradiated in air with low-energy protons. A micro beam is used to test and evaluate of the technique. The imaging setup is used direct in-line transmitted geometry. The proof-of-principle and method of image contrast are based on high-resolution analysis of single particle tracks in the pixel detector [10]. We examine the capability to produce contrast images from detailed pattern recognition and spectral tracking morphology analysis of the single particle tracks depending on the deposited energy, size (number of pixels) and energy height of the pixelated signals [11]. Spatial maps can be thus produced of particle energy loss across the sample [10] with high-resolution, enhanced contrast and low dose. Radiographies of event rate are also produced which serve for derivation of total fluency and deposited dose.

## 2 Methods and materials

### 2.1 Pixel detector Timepix3, deposited energy contrast imaging

We use the pixel detector Timepix3 [9] equipped with a  $500\ \mu\text{m}$  Si sensor. The detector provides a high-granularity matrix of energy-sensitive pixels ( $256 \times 256$  pixels). The pixel pitch size is  $55\ \mu\text{m}$  for a total sensitive area of  $14.08\ \text{mm} \times 14.08\ \text{mm} = 1.98\ \text{cm}^2$ . The detector is operated and readout with the fast data-rate AdvaPIX interface. Data are readout in continuous pixel stream data driven mode including acquisition visualization online with the PIXET software tool. The detector sensor surface has a thin non-sensitive is coated layer (about  $1\ \mu\text{m}$ , Aluminium) which makes the sensor also non-sensitive to light.

The principle of density-sensitive contrast imaging is based on the precise measurement of small changes in the proton deposited energy [3-6, 10]. This method requires a well-defined (monoenergetic, collimated/scanning, parallel) beam together with a spectral sensitive position-sensitive detector [5]. The initial energy of the accelerated protons (2.9 MeV in this work) is known and changes of proton deposited energy after passing sample are accurately measured by the pixel detector. Each particle makes a characteristic trace in the pixel detector consisting of various pixels called a cluster [5, 11]. The micro-scale cluster morphology and spectral response of the track is correlated with the deposited

energy [11]. Raw data are converted to energy using a per-pixel calibration [12]. The transmitted protons are registered in high spatial resolution by the detector with sub-pixel (detector pixel pitch size  $55\ \mu\text{m}$ ) resolution [5]. Position resolution up to few  $\mu\text{m}$  level is made possible by pattern recognition and charge sharing model fitting [5]. The imaging contrast principle requires few particles per imaging bin.

Contrast imaging can be derived from spectral-tracking parameters of the registered pixelated clusters [10]. Several of these pattern-recognition parameters are correlated with the deposited energy. The parameters which we examine in this work are: deposited energy, cluster area size and cluster per-pixel height of single particle track. Event counts of localized protons in the given imaging bin are also evaluated. The deposited energy is given by the sum of all per-pixel energy values of the cluster. Cluster area size is the number of cluster pixels; cluster per-pixel height corresponds to the maximum energy value of the pixels in the given cluster.

## 2.2 Measuring setup, geometry

Measurements were performed at the Tandetron 4130 MC accelerator. The pixel detector was scanned in air with a proton micro beam of energy 2.9 MeV. The detector and sample were placed in air perpendicular to the beam axis. The distance between the accelerator beam nozzle and the detector sensor was 7 mm, (the setup is shown in Fig. 1).

The imaged samples were held by plastic frames of larger size. The samples on the frames were mounted in close geometry in front of the detector. The detector and sample were mounted on a movable sample holder, which was used for spatial scanning of large samples. Small homogeneous samples were irradiated using the automatic beam scanning system, which covered a square field of  $1.5 \times 1.5\ \text{mm}^2$ .

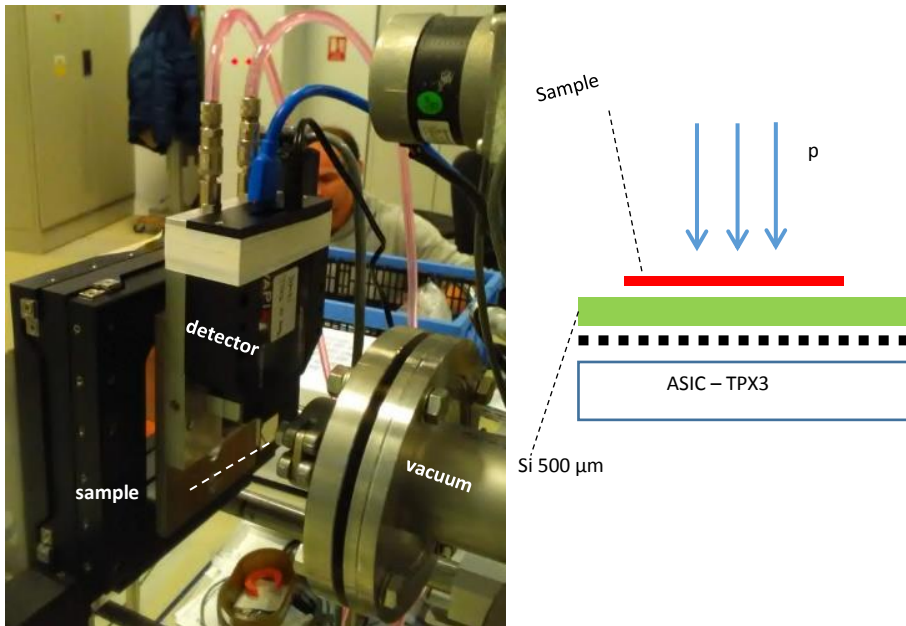


**Fig. 1.** Photo (left) and scheme (right) of the imaging setup in air. The detector is placed at a distance of 7 mm from the accelerator beam nozzle. The deposited energy and position of the transmitted protons are registered in high-resolution by a Timepix3 detector with a  $500\ \mu\text{m}$  silicon sensor (shown in green).

**Table 1.** Imaging samples used. Composition, labels, foil thickness are given.

Label	Sample, composition and size	Composition, layout
A	No sample	Air
B	Mylar foil 5 $\mu\text{m}$	Homogenous sample, one foil
C	Al foil 5 $\mu\text{m}$	Homogenous sample, one foil
D	Stairs of Al foils	Stacked sample, stairs of foils with total thicknesses 0, 5, 10, 15, 25 and 30 $\mu\text{m}$
E	Stairs of Mylar foils	Stacked sample, stairs of 5 $\mu\text{m}$ foils, with total thicknesses from 0 to 20 $\mu\text{m}$
F	Edge of metallic Mylar foil	Edge of the foil is in the middle of a scanned area, the metallic layer starts approximately 1 mm next to the edge of foil
G <sub>1</sub>	Metal grid 0.25 mm	Grid placed directly on the exit window
G <sub>2</sub>		Same grid, rotated at other angle

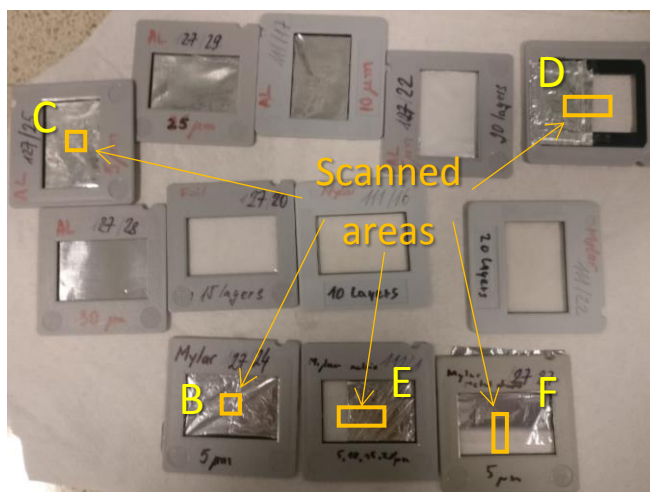


**Fig. 2.** Imaging samples used: simple Mylar foil 5  $\mu\text{m}$  (B); simple Aluminium foil 5  $\mu\text{m}$  (C); stair of Aluminium foil (0, 5, 10, 15, 25 and 30  $\mu\text{m}$ ) (D); stairs of Mylar foil (0, 5, 10, 15 and 20  $\mu\text{m}$ ) (E); edge of 5 $\mu\text{m}$  Mylar foil (F). Orange rectangles and squares represent the scanned areas.

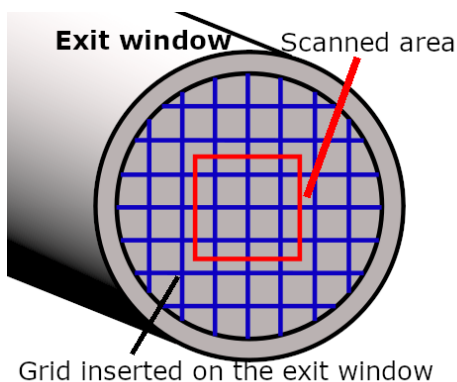


**Fig. 3.** Scheme of the metallic grid sample (G<sub>1</sub> and G<sub>2</sub>) placed closely on the exit window. The beam scanned area is illustrated (red square).

## 2.3 Imaged samples

Well-defined samples were assembled from layers of thin Mylar and Aluminium foils as well as a thin metallic grid to serve as evaluating imaging samples. The detector was also irradiated without sample in order to examine the beam spectral and beam size profile homogeneity. The sample list is given in Table 1. Several samples are shown in Fig. 2. The grid sample is illustrated in Fig. 3.

## 3 Measurements and image processing

### 3.1 Data acquisition, data processing

Samples were imaged with a low intensity beam (flux  $\approx 10^3$  protons/cm<sup>2</sup>/s). A low intensity beam ( $< 10^{-13}$  A/cm<sup>2</sup>) is required for detailed event-by-event detection in the pixel detector [11]. This acquisition mode allows registering and analysing in detail the single particle tracks for precise high-resolution spectrometry (deposited energy). Collected raw data are processed offline starting with the application of the per-pixel calibration and pattern recognition and identification of pixelated clusters. Detailed event lists are produced with spectral, tracking, position and time information. For each event the position in  $X$  and  $Y$  fitted coordinates of the cluster centroid is determined with sub-pixel  $\mu\text{m}$  level resolution [4]. Also deposited energy, maximum per-pixel energy value (height) of the cluster, number of pixels (area) and further spectral-tracking pattern recognition parameters such as cluster roundness and linearity are registered [11].

Radiographies can be produced in the form of spatial distribution of these parameters including the event count radiograph. The image spatial bin of the given radiograph can be scaled in proportion to the event fluency to e.g., the detector pixel size i.e., 55  $\mu\text{m}$ , or smaller e.g., 10  $\mu\text{m}$  [9]. The information produced is namely the material density map of the imaged sample. The sensitivity and dynamic range of the image contrast information are given by the value and extent of the selected cluster parameter. If multiple events of cluster centroids located in the same image bin, the average or maximum value are evaluated and displayed. Proton radiographies have been made for all samples using the selected parameters (counts, deposited energy, cluster area and heights). For these quantities the average or the maximum value are evaluated. Resulting radiographies can be produced from all events i.e., all clusters or from filtered data. Data are filtered in dependence to the individual parameters and their combinations.

### 3.2 Proton radiographies

Radiographies of the 5  $\mu\text{m}$  Al foil stack (sample D) imaged by a 2.9 MeV proton scanning micro beam is shown in Fig. 4. The image shown is produced with spatial bin equal to the detector pixel size (55  $\mu\text{m}$ ). In the data a basic filter was applied (clusters greater than 7 px size), which corresponds to protons both primary beam as well as scattered and beam halo protons. This filter removes non-proton events, such as X rays and unwanted or background electrons. For the same data set are shown four radiographies of different contrast response each produced by evaluation of different cluster parameter. Information is derived on the energy loss of the probe particle and material composition density map across the imaged sample. The image exhibits a main central component, resulting from the primary beam non-scattered particles in the scanning microbeam. In the periphery there is a small component of decreasing radial intensity. Consisting of scattered particles this periphery halo component can be resolved also by the deposited energy which is nearly half that of

non-scattered primary beam particles (see Fig. 4a, c). The evaluation and quantification of this and further effects observed are subject of future work.

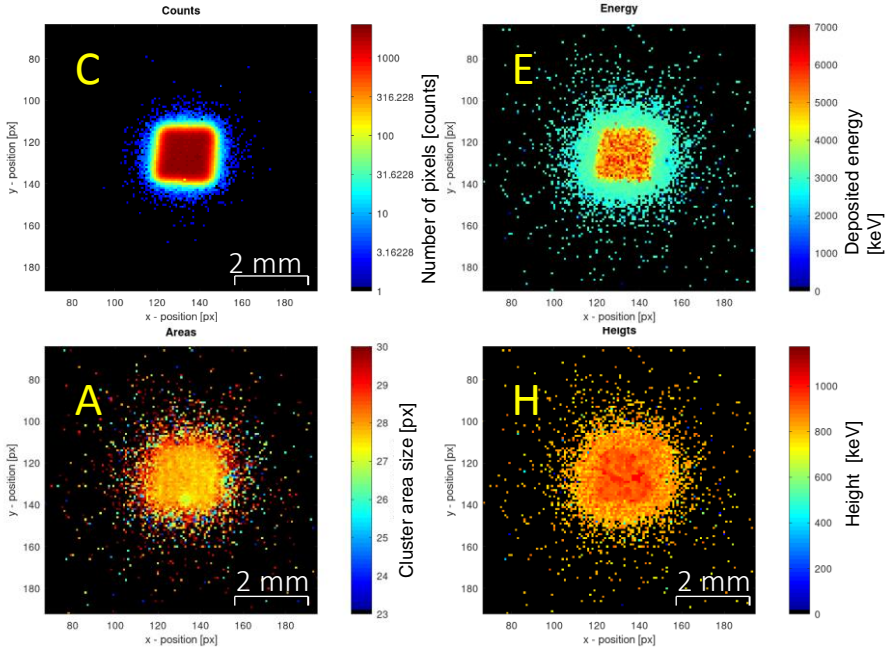


**Fig. 4.** Proton radiographies of sample C with 2.9 MeV protons measured by a Timepix3 500  $\mu\text{m}$  silicon sensor detector. The images are based on event count (C), deposited energy (E), cluster area sizes (A) and cluster height (H). All images are made from the same set of filtered data (filter used:  $A > 7$  px). The spatial bin is equal to the detector pixel size (55  $\mu\text{m}$ ).

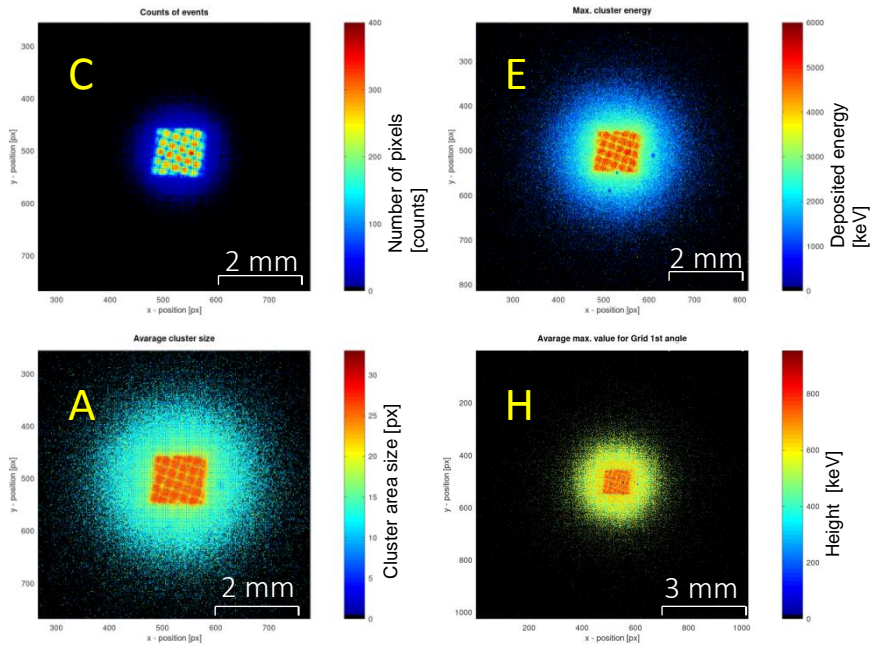


**Fig. 5.** Similar to Fig. 4 showing proton radiographies of sample  $G_1$ . Images are made from all data (no filtering applied). Image produced with subpixel resolution (one spatial bin corresponds to 13.75  $\mu\text{m}$ ).

Depending on the total event fluency, i.e., total number of particles registered, it is possible to image radiographies with varying spatial resolution. A radiograph with subpixel resolution is shown in Fig. 5 of the grid sample (sample G1) whose scheme is illustrated in Fig. 3. Four radiographies of different contrast response are shown. In the images presented, no event filter was applied.

Radiographies with enhanced contrast can be produced by combining filtered data with non-filtered data i.e., the image of all cluster events, see Fig. 6. Structures of the same material and small thickness down to the  $\mu\text{m}$  range can be resolved.

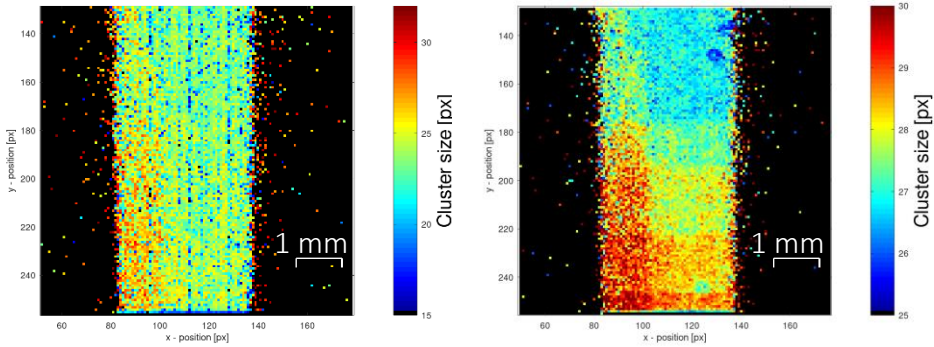


**Fig. 6.** Proton radiographies produced from non-filtered i.e., all data (left) and filtered data (right). The sample E is imaged with 2.9 MeV protons. The right filtered image is made from events selected in the following range: Deposited energy from 0.8 to 3.6 MeV, cluster area greater than 10 px and cluster energy height greater than 300 keV. Radiographies shown in spatial bin of one detector pixel i.e., 55  $\mu\text{m}$ .

### 3.3 Evaluation of the Technique

This technique sensitivity allows resolving materials of thickness at the  $\mu\text{m}$  level in wide dynamic range limited by the range of the charged particle used across the sample. The maximum thickness size of imaged samples with 2.9 MeV protons is several tens of  $\mu\text{m}$  depending on the material density. The contrast principle of this technique allows even just one particle to be required per spatial bin. Depending on the flux used ( $< 10^5$  particles/ $\text{cm}^2/\text{s}$ ), selected spatial resolution (achieved down to the few  $\mu\text{m}$  level) and overall image sample area size, complete scans can be performed in few seconds up to few minutes. The counting statistics which depend on the chosen spatial resolution are summarized in Table 2. Values given for the lowest statistics (i.e., on average one particle per spatial bin). Estimated typical values of total dose given to the sample are included. These values are calculated for a mean deposited dose in the sample of 200  $\mu\text{Gy}$  per proton.

**Table 2.** Lowest event count statistics depending on the spatial resolution. Values given for a minimal event rate of 1 proton per imaging bin (spatial resolution) for a sample of size 10 mm  $\times$  10 mm. Scanning time given for a particle flux of  $1 \times 10^4$  protons/ $\text{cm}^2/\text{s}$ . Total dose values are included.

Number of particles	Spatial bin size	Scanning time	Total dose
$3.3 \times 10^4$	1 bin $\approx$ 1 px $\approx$ 55 $\mu\text{m}$	3.3 s	6.6 $\mu\text{Gy}$
$1 \times 10^6$	1 bin $\approx$ 10 $\mu\text{m}$	100 s	200 $\mu\text{Gy}$
$4 \times 10^6$	1 bin $\approx$ 5 $\mu\text{m}$	400 s	800 $\mu\text{Gy}$

## 4 Conclusions

Use of a spectral and imaging detector such as Timepix3 enables to apply the technique of deposited energy sensitive radiography using standard proton beams in air. Even a standard radionuclide alpha source can be used (limited contrast, limited count rate). We evaluated and tested the detector resolving power on well-defined thin samples using a mono-energetic collimated proton micro beam. We examined the image contrast response on various parameters of the single particle tracks in the pixel detector. These can be combined to refine further the image contrast and provide information on the sample material composition (subject of future work). The spatial resolution of the resulting radiographs is in the range 55  $\mu\text{m}$  (detector pixel size) to 5  $\mu\text{m}$  (limit by the detector resolution and beam straggling in air) depending also on the event rate (total particle fluency). Thanks to the detector high sensitivity the event rate per imaged spatial bin can be even one particle per pixel. Structures of similar and even of the same material can be resolved down to small thickness in the  $\mu\text{m}$  range. The achieved resolution and single particle sensitivity enable to minimize the radiation dose and resolve composition and details hard to achieve with conventional or other non-destructive techniques. The technique allows to resolve components in the transmitted beam such as scattered particles forming a periphery halo. Quantification and evaluation of distortion of the resulting image are in progress. Future work includes combined evaluation of multi-parametric radiography and further contrast enhancement by data post-processing techniques. The imaging sensitivity can be further improved by measurements in vacuum. Higher sensitivity can be provided by use of heavier particles such as  $^{12}\text{C}$  ions.

The authors appreciate the remarks and valuable suggestions given by the reviewers. Measurements were carried out at the CANAM infrastructure of the NPI CAS Rez supported through MŠMT project No. LM2015056.

## References

1. A. M. Koehler, *Science* **160** (1968)
2. R.P. Johnson, *Rep. Prog. Phys.* **81**, 1 (2018)
3. I.F. van Maanen, et. al., *NIM-B* **113**, 382-386 (1996)
4. R. Ortega, et. al., *NIM-B* **181**, 475-479 (2001)
5. J. Jakubek, A. Cejnarova, T. Holy et al., *NIM-A* **591**, 155-158 (2008)
6. J. Jakubek, *JINST* **4**, P03013 (2009)
7. O. Romanenko, V. Havranek, A. Mackova et al., *Rev Sci Instrum.* **90**, 013701 (2019)
8. A. Mackova, P. Malinsky, M. Cutroneo et al., *Eur. Phys. J.+* **136**, 5, 558 (2021)
9. T. Poikela, J. Plosila, T Westerlind, et al., *JINST* **9**, C05013 (2014)
10. V. Olsansky, C. Granja, C. Oancea et al., *JINST* (2021) *submitted*
11. C. Granja, J. Jakubek, S. Polansky et al., *NIM-A* **908**, 60-71 (2018)
12. J. Jakubek, *NIM-A*, **633**, S262-S266 (2011)